THE JOURNAL OF BIOLOGICAL CHEMISTRY
Vol. 279, No. 26, Issue of June 25, pp. 27502–27510, 2004

Printed in U.S.A.

Solution Structures of a Cyanobacterial Metallochaperone

INSIGHT INTO AN ATYPICAL COPPER-BINDING MOTIF*[S]

Received for publication, February 24, 2004, and in revised form, April 5, 2004
Published, JBC Papers in Press, April 8, 2004, DOI 10.1074/jbc.M402005200

Lucia Banci‡, Ivano Bertini‡§, Simone Ciofi-Baffoni‡, Xun-Cheng Su‡, Gilles P. M. Borrelly¶, and Nigel J. Robinson¶‖

From the ‡Magnetic Resonance Center CERM and Department of Chemistry, University of Florence, Via Luigi Sacconi 6, 50019 Sesto Fiorentino, Florence, Italy and ¶Cell and Molecular Bioscience, Medical School, University of Newcastle, NE2 4HH, United Kingdom

The Atx1 copper metallochaperone from *Synechocystis* PCC 6803, ScAtx1, interacts with two P_1-type copper ATPases to supply copper proteins within intracellular compartments, avoiding ATPases for other metals *en route*. Here we report NMR-derived solution structures for ScAtx1. The monomeric apo form has a $\beta\alpha\beta\beta\alpha$ fold with backbone motions largely restricted to loop 1 containing Cys-12 and Cys-15. The tumbling rate of Cu(I)ScAtx1 (0.1–0.8 mM) implies dimers. Experimental restraints are satisfied by symmetrical dimers with Cys-12 or His-61, but not Cys-15, invading the copper site of the opposing subunit. A full sequence of copper ligands from the cell surface to thylakoid compartments is proposed, considering *in vitro* homodimer liganding to mimic *in vivo* liganding in ScAtx1-ATPase heterodimers. A monomeric high resolution structure for Cu(I)ScAtx1, with Cys-12, Cys-15, and His-61 as ligands, is calculated without violations despite the rotational correlation time. $^2J_{NH}$ couplings in the imidazole ring of His-61 establish coordination of $N^{\epsilon 2}$ to copper. His-61 is analogous to Lys-65 in eukaryotic metallochaperones, stabilizing $Cu(I)S_2$ complexes but by binding Cu(I) rather than compensating charge. Cys-Cys-His ligand sets are an emergent theme in some copper metallochaperones, although not in related Atx1, CopZ, or Hah1. Surface charge (Glu-13) close to the metal-binding site of ScAtx1 is likely to support interaction with complementary surfaces of copper-transporting ATPases (PacS-Arg-11 and CtaA-Lys-14) but to discourage interaction with zinc ATPase ZiaA and so inhibit aberrant formation of copper-ZiaA complexes.

Most of the biosphere is either directly, or indirectly, reliant upon effective copper delivery to the thylakoids of primary producers. The conversion of light into useful chemical energy by cyanobacteria and plants involves the transfer of electrons within the thylakoid lumen between two membranous photosystems. Electrons are commonly transferred via plastocyanin-bound copper. Plastocyanin is located within the thylakoid lumen and is imported as an unfolded protein (1), necessitating a separate copper supply in order to form the holoenzyme.

Analyses of mutants of the cyanobacterium *Synechocystis* PCC 6803 established that two copper-transporting P_1-type ATPases, PacS and CtaA, plus a small soluble copper metallochaperone, Atx1 (herein referred to as ScAtx1), are required for normal photosynthetic electron transfer via plastocyanin and for the activity of a second thylakoid-located copper protein, a caa_3-type cytochrome oxidase (2, 3). In common with related polypeptides from other bacteria, yeast, and man (4–7), ScAtx1 directly interacts with soluble amino-terminal domains of P_1-type copper ATPases (3). However, unlike other copper metallochaperones, ScAtx1 from *Synechocystis* PCC 6803 associates with two such proteins, and there is a presumption that the vectors for copper transfer alternate in each of these two interactions. In *Synechococcus* PCC 7942, PacS is located in thylakoid membranes (8), whereas CtaA is thought to import copper at the plasma membrane (9). The phenotypes of Δ*ctaA* and Δ*pacS* mutants of *Synechocystis* PCC 6803 are consistent with both ATPases transporting copper in an inward direction into the cytosol and then into the thylakoid lumen (3). This provides an attractive system for studying the process of copper transfer between a copper metallochaperone and its partners. In addition to PacS and CtaA, *Synechocystis* PCC 6803 also contains a P_1-type ATPase, ZiaA, that transports zinc and not copper (10) and has an amino-terminal domain with higher affinity for copper than for zinc (11). A subdomain of ZiaA ($ZiaA_N$) is predicted to form a ferredoxin-like fold analogous to the amino-terminal regions of the two copper transporters, but ScAtx1 gave no detectable two-hybrid interaction with this subdomain of ZiaA (11) nor with the entire soluble amino-terminal region of ZiaA (3). Provided there is no freely available cytosolic copper in *Synechocystis* PCC 6803, as implied for *Escherichia coli* (12), lack of an ScAtx1-$ZiaA_N$ interaction will impose a kinetic barrier to discourage formation of otherwise thermodynamically favored copper-$ZiaA_N$ complexes (11) while copper traffics to the thylakoid. What are the surfaces of ScAtx1 that allow interaction with the copper transporters but not with ZiaA?

There is considerable interest in understanding the submolecular processes by which copper is passed between partner proteins in cellular trafficking pathways to avoid intracellular metal release. NMR-derived solution structures revealed that loop 1, containing Cys ligands, and loop 5, containing Lys-65, of yeast Atx1 are dynamic during interaction with its cognate

* This work was supported by the European Community Grant SPINE QLG2-CT-2002-00988, ("Structural Proteomics in Europe") and by MIUR COFIN 2003 "Il Ruolo degli Ioni Metallici nei Processi Metabolici." The costs of publication of this article were defrayed in part by the payment of page charges. This article must therefore be hereby marked "*advertisement*" in accordance with 18 U.S.C. Section 1734 solely to indicate this fact.

The atomic coordinates and structure factors (code 1SB6) have been deposited in the Protein Data Bank, Research Collaboratory for Structural Bioinformatics, Rutgers University, New Brunswick, NJ (http://www.rcsb.org/).

[S] The on-line version of this article (available at http://www.jbc.org) contains Tables 1 and 2 and Figs. 1–5.

§ To whom correspondence should be addressed: CERM and Dept. of Chemistry, University of Florence, Via L. Sacconi 6, 50019 Sesto Fiorentino, Florence, Italy. Tel.: 39-055-4574272; Fax: 39-055-4574271; E-mail: bertini@cerm.unifi.it.

‖ Supported by the Biotechnology and Biological Sciences Research Council.

ATPase, apoCcc2. It has been proposed that the observed flexibility in loops 1 and 5 of yeast apoAtx1 may provide a trigger for copper release and allow the chaperone to adapt to its two partners, downstream of CTR1 and upstream of Ccc2 (7). Loop 1 of copper-CopZ from *Bacillus subtilis* assumes the conformation of apo- rather than copper-CopZ upon contact with the amino-terminal domain of CopA (4). This implies copper release from the metallochaperone to the exporter, and Δ*copZ* mutants were subsequently shown to be copper-sensitive (5), consistent with a role in export rather than import. It is presumed that any analogous mechanism for ScAtx1 must be somehow adapted to encourage copper transfer to the metallochaperone from one P_1-type ATPase as well as release to another. The copper coordination sphere of ScAtx1 was probed with EXAFS,[1] and 108 NOE-derived distance restraints in the region of presumptive loops 1 and 5 were used to analyze the spatial arrangement of residues in this region (13). This supported copper binding to Cys-15 and Cys-12 from loop 1 plus His-61 from loop 5, with all NMR-refined models orientating these three residues at distances compatible with a trigonal copper (I) site. Conversion of His-61 to Arg altered two-hybrid interactions with PacS, but not with CtaA, implying that the interacting surfaces of the two ATPases are not identical in these regions (13).

Here we show copper liganding to $N^{\epsilon 2}$ of His-61. The full structure of ScAtx1 is reported as a prelude to direct analyses of ScAtx1 complexes with PacS and CtaA and to identify features that account for noninteraction with the analogous amino-terminal domain of ZiaA. We establish that metal-loaded ScAtx1 forms dimers *in vitro* and that Cys-15 alone does not enter the copper site of the opposing monomer consistent with Cys-12 thiols and His-61 $N^{\epsilon 2}$ commencing and/or concluding ligand exchange with PacS and CtaA. Flexibility in the region of loop 1 of apoScAtx1 is suggestive of Cys-12, rather than His-15, being the pioneer ligand during copper transfer from CtaA and allowing a model to be generated for the entire copper ligand sequence from the cell surface to the thylakoid.

EXPERIMENTAL PROCEDURES

ScAtx1 Protein Expression and Purification—E. coli cells (BL21 (DE3)) were grown in Luria-Bertani or minimal media containing M9 salts. All buffers were prepared using Milli-Q deionized water. HEPES and Tris buffer salts were obtained from Melford Laboratories Ltd. and Roche Applied Science. Chromatography materials were purchased from Amersham Biosciences, and other reagents were obtained from Sigma. Plasmid pETATX1, for overexpression of ScAtx1, was generated as described previously (3), and recombinant protein produced in *E. coli* (BL21(DE3)) was exposed to copper (0.5 mM) in LB medium. Lysates (2.5 ml) were applied to Sephadex G-75 (2.5 × 50 cm), and fractions (5 ml) eluted in 25 mM Tris-HCl, pH 7.0, were analyzed for total protein and for copper by atomic absorption spectroscopy. Pooled copper peak fractions were applied to Q-Sepharose and sequentially eluted with 25 mM Tris-HCl, pH 7.0, followed by 0.7 M NaCl, 25 mM Tris-HCl, pH 7.0. Fractions were again analyzed for copper and protein, and copper-containing fractions were desalted on Sephadex G-25 in 25 mM Tris-HCl, pH 7.0. A single prominent band of the anticipated size was detected by PAGE, and the amino-terminal 10 residues of sequence (Beckman LF 3000 protein sequencer) previously confirmed the identity of this purified protein (3). ^{15}N-Labeled ScAtx1 was prepared from cells grown in minimal medium containing M9 salts supplemented with $^{15}NH_4Cl$ and exposed to copper (0.02 mM).

Purified polypeptide was incubated with 10 mM dithiothreitol, transferred to an N_2 atmosphere chamber, and fractionated on Sephadex G-25 equilibrated in and eluted with hydrochloric acid, pH 2.0, with no added reductant. If pre-metalated protein was required, recovered material was exposed to an equivalent molar concentration of copper(I) chloride prior to the addition of 1 M HEPES, pH 7.0. (Some apo samples were prepared without addition of copper at this stage, but copper(I) was subsequently added to the final concentrated protein at pH 7.0.) Samples were further concentrated by passage through Q-Sepharose, sequentially washed with 25 mM HEPES, pH 7.0, followed by 0.7 M NaCl, 25 mM HEPES, pH 7.0. Fractions were again analyzed for protein, and selected fractions were desalted on Sephadex G-25, eluted with 50 mM sodium phosphate buffer, pH 7.0, 10% D_2O. Copper content was finally checked through atomic absorption spectroscopy. Analytical gel filtration was performed on a Superdex 75 10/30 HR sizing column in 50 mM sodium phosphate buffer, pH 7, containing, when specified, 1.5 mM dithiothreitol. *S. cerevisiae* Ccc2a domain is available in our laboratory.

NMR Experiments and Structure Calculations—NMR spectra were performed on Avance 800, 600, and 500 Bruker spectrometers operating at proton nominal frequencies of 800.13, 600.13, and 500.13 MHz, respectively. All the triple resonance (TXI 5-mm) probes used were equipped with pulsed field gradients along the *z* axis. The 500-MHz machine was equipped with a triple resonance cryoprobe.

The NMR experiments were recorded on ^{15}N-labeled and unlabeled samples. Two-dimensional TOCSY (14) spectra were recorded on the 600-MHz spectrometers with a spin-lock time of 100 ms, a recycle time of 1.5 s, and a spectral window of 15 ppm. Two-dimensional NOESY maps (15, 16) were acquired on the 800-MHz spectrometers with a mixing time of 100 ms, a recycle time of 1.5 s, and a spectral window of 15 ppm. The two-dimensional ^{15}N-^{1}H HSQC (17) maps and three-dimensional NOESY-^{15}N HSQC experiments (100-ms mixing time) (18, 19) were obtained at 800 MHz with an INEPT delay of 2.6 ms, a recycle time of 1.5 s, and spectral windows of 15 and 40 ppm for the ^{1}H and ^{15}N dimensions, respectively. HNHA experiments (20) were performed at 800 or 500 MHz to determine $^3J_{HNH\alpha}$ coupling constants. HNHB experiments (21) were performed at 500 MHz. To identify the coordination mode of copper(I)-binding histidine, a ^{15}N HSQC experiment was performed for measuring $^2J_{N\epsilon H\delta}$, $^2J_{N\epsilon H\epsilon}$, $^2J_{N\delta H\epsilon}$, and $^3J_{N\delta H\delta}$ coupling constants (22). In this experiment, the INEPT delay was set to 22 ms. All three-dimensional and two-dimensional spectra were collected at 298 K, processed with the standard Bruker software (XWINNMR), and analyzed with the XEASY program (23).

The backbone assignment has been performed using the three-dimensional ^{15}N NOESY-HSQC, two-dimensional NOESY, and two-dimensional TOCSY spectra. Consequently, the combination of three-dimensional ^{15}N NOESY-HSQC, HNHA, and HNHB and two-dimensional NOESY and TOCSY spectra allows the resonances assignment of side chains. Distance constraints for structure calculation were obtained from three-dimensional ^{15}N NOESY-HSQC, two-dimensional NOESY experiments. $^3J_{HNH\alpha}$ coupling constants, stemmed from HNHA experiments, were transformed through the Karplus equation into backbone dihedral ϕ angle constraints for structural calculations. The elements of secondary structure were determined on the basis of the $^3J_{HNH\alpha}$ coupling constants and of the backbone NOEs from three-dimensional ^{15}N NOESY-HSQC and two-dimensional NOESY spectra.

An automated CANDID approach combined with DYANA torsion angle dynamics algorithm (24) was used to assign the ambiguous NOE cross-peaks and to have a preliminary apo- and monomeric Cu(I)ScAtx1 structure. Structure calculations were then performed through iterative cycles of DYANA (25) followed by restrained energy minimization (REM) with AMBER 5.0 (26) applied to each member of the family. Homodimeric Cu(I)ScAtx1 structure calculations were performed using the program DYANA (25), and the 20 conformers with the lowest target function were minimized through AMBER 5.0 program package (26). The copper ion was included in the structure calculations of the copper(I)-loaded monomeric and dimeric forms following the same procedure already used for the monomeric and dimeric superoxide dismutase (27). The sulfur atoms of Cys-12 and Cys-15 and $N^{\epsilon 2}$ of the imidazole ring of His-61 were linked to the metal ion through upper distance limits of 2.5 and 2.2 Å, respectively. This approach does not impose any fixed orientation of the ligands with respect to the copper(I) ion.

The quality of the structures was evaluated using the programs PROCHECK-NMR (28). The figure was generated with the program MOLMOL (29). The atomic coordinates of apoScAtx1 have been deposited in the Protein Data Bank (code 1SB6).

Relaxation Measurements and Analysis—Relaxation experiments were performed on Bruker Avance 600-MHz spectrometers at 298 K, and the protein sample concentrations range from 0.8 to 0.1 mM. ^{15}N R_1, R_2, and steady-state heteronuclear NOEs were measured with pulse sequences as described by Farrow *et al.* (30). R_2 values were measured as a function of refocusing times (τ_{CPMG}) ranging from 450 to 1150 μs

[1] The abbreviations used are: EXAFS, extended x-ray absorption fine structure; NOE, nuclear Overhauser effect; NOESY, nuclear Overhauser effect spectroscopy; r.m.s.d., root mean square deviation; DTT, dithiothreitol; TOCSY, total correlation spectroscopy; REM, restrained energy minimization.

TABLE I

Statistical quality analysis of the REM family and of the mean structure of apoScAtx1 from Synechocystis PCC 6803

REM means the energy minimized ensemble of 20 structures, ⟨REM⟩ is the energy minimized average structure of the ensemble.

RSM violations per experimental distance constraint (Å)[a]	REM (20 structures)	⟨REM⟩
Intraresidue (204)	0.0148 ± 0.0021	0.0153
Sequential (299)	0.0080 ± 0.0017	0.0097
Medium range[b] (241)	0.0115 ± 0.0027	0.0151
Long range (273)	0.0134 ± 0.0019	0.0110
Total (1017)	0.0120 ± 0.0011	0.0125
ϕ (44) (deg)	0	0
Average number of violations per structure		
Intraresidue	4.65 ± 1.65	2
Sequential	2.75 ± 0.88	5
Medium range[b]	4.90 ± 1.4	3
Long range	6.70 ± 1.62	4
Total	19.00 ± 3.00	14
ϕ	0.2 ± 0.05	0
Average no. of NOE violations larger than 0.3 Å	0	0
Total NOE square deviations (Å^2)	0.15 ± 0.06	0.15
Average torsion deviations (rad^2)	0.02 ± 0.01	0
r.m.s.d. to the mean structure (3–64) (Å)	0.49 ± 0.12 Å (BB) 0.83 ± 0.14 (HA)	
Structural analysis[c]		
% of residues in most favorable regions	75.5	74.6
% of residues in allowed regions	21.4	20.3
% of residues in generously allowed regions	2.8	3.4
% of residues in disallowed regions	1.0	1.3
H-bond energy (kJ mol^{-1})	3.63 ± 0.12	3.63
Overall *G*-factor	−0.22 ± 0.02	−0.30

[a] The number of experimental constraints for each class is reported in parentheses.
[b] Medium range distance constraints are those within residues (i,i + 2), (i,i + 3), (i,i + 4), and (i,i + 5).
[c] Data resulted from the Ramachandran plot analysis over the assigned residues. In the PROCHECK statistics, the average hydrogen-bond energy within 2.5–4.0 kJ mol^{-1} and overall *G*-factor over −0.5 is expected to be a good quality structure.

with the Carr-Purcell-Meiboom-Gill (CPMG) sequence (31, 32) to identify backbone conformational exchange. In all experiments the water signal was suppressed with the "water flipback" scheme (33). R_1 and R_2 experiments were acquired with 8 or 16 scans, whereas {^{1}H}-^{15}N NOE spectra were acquired with 48 scans. Duplication of measurements was performed to estimate the experimental uncertainty. A recycle delay of 3 s was used for R_1 and R_2 relaxation experiments except for the NOE experiments in which the recycle delay was 5 s. A total of 2048 K (^{1}H) × 128 (^{15}N) data points were collected. All spectra were processed with the XWINNMR program (Bruker) and analyzed with Sparky software (T. D. Goddard and D. G. Kneller, University of California, San Francisco).

NMR relaxation data were fitted with the routine procedure implemented in the Sparky program. A search routine was used within Sparky to find the positions of the peak maxima. The exponential decay curves for R_1 and R_2 peak intensities were fitted to the two-parameter curve, $h = A \times \exp(-R \times t)$, where h is height and t is the variable delay parameter. The heteronuclear NOE values were obtained from the ratio of the peak intensity for ^{1}H-saturated and unsaturated spectra. The error was estimated from 500 different fit trials, and peaks that had an error superior to 20% were not considered in the analysis. The experimental relaxation rates were used to map the spectral density function values, $J(\omega_H)$, $J(\omega_N)$, and $J(0)$, following a procedure available in the literature (34).

The overall rotational correlation time (τ_m) values were estimated from the R_2/R_1 ratio (35). The diffusion tensor of the molecule was estimated by fitting the local correlation times for the NH vector of each residue to an input structure with the program quadric_diffusion, available from the website of A. G. Palmer III (see Ref. 36). In this analysis, care was taken to remove from the input relaxation data those NHs having an exchange contribution to the R_2 value or exhibiting large amplitude internal motions on a time scale longer than a few hundred picoseconds, identified from low NOE values, as inclusion of these data would bias the calculated tensor parameters (37, 38). The input structures for quadric_diffusion were the energy-minimized average solution structures of monomeric apoScAtx1 and monomeric/dimeric Cu(I)ScAtx1.

RESULTS

Solution Structure and Mobility of apoScAtx1—The ^{15}NHSQC spectrum of the apo form of ScAtx1 (64 amino acids) shows a good dispersion of the signals indicating that the protein is in a folded state. Assignments of the resonances of apoScAtx1 started from the analysis of the ^{1}H-^{15}N HSQC maps that allowed the identification of the ^{15}N and ^{1}HN resonances. Analysis of ^{15}N-edited three-dimensional NOESY-HSQC and of two-dimensional NOESY and TOCSY maps allowed sequence-specific assignment. 57 of the expected 63 ^{15}N backbone amide resonances were observed and assigned. The backbone NH resonances are missing for residues Met-1, Thr-2, Ala-11, Cys-12, Glu-13, and Ala-14. Totally, the resonances of 95% of nitrogen atoms and 96% of protons were assigned. The ^{1}H and ^{15}N resonance assignments of the apo form are reported in supplemental Table 1.

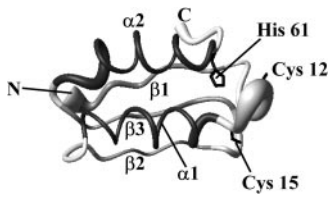

FIG. 1. **Solution structure of apoScAtx1; the side chains of His-61, Cys-12, and Cys-15 are shown.** The secondary structure elements are shown: β-strands in *gray* and helices in *black*. The radius of the tube is proportional to the backbone r.m.s.d. value of each residue.

2100 NOE cross-peaks have been assigned and integrated, providing 1118 unique upper distance limits, of which 1017 are meaningful. 44 ϕ angles derived from a HNHA experiment were also used in structure calculations. After restrained energy minimization with AMBER program on each of 20 lowest target function structures, obtained from DYANA calculations, the root mean square deviation (r.m.s.d.) for protein backbone and heavy atoms to the mean structure (for residues 3–64) is 0.49 Å (with a variability of 0.12 Å) and 0.83 Å (with a variability of 0.14 Å), respectively. The penalties for distance constraints and angle constraints are 0.15 ± 0.06 Å^2 and 0.02 ± 0.01 radians^2, respectively. The statistical analyses of the REM

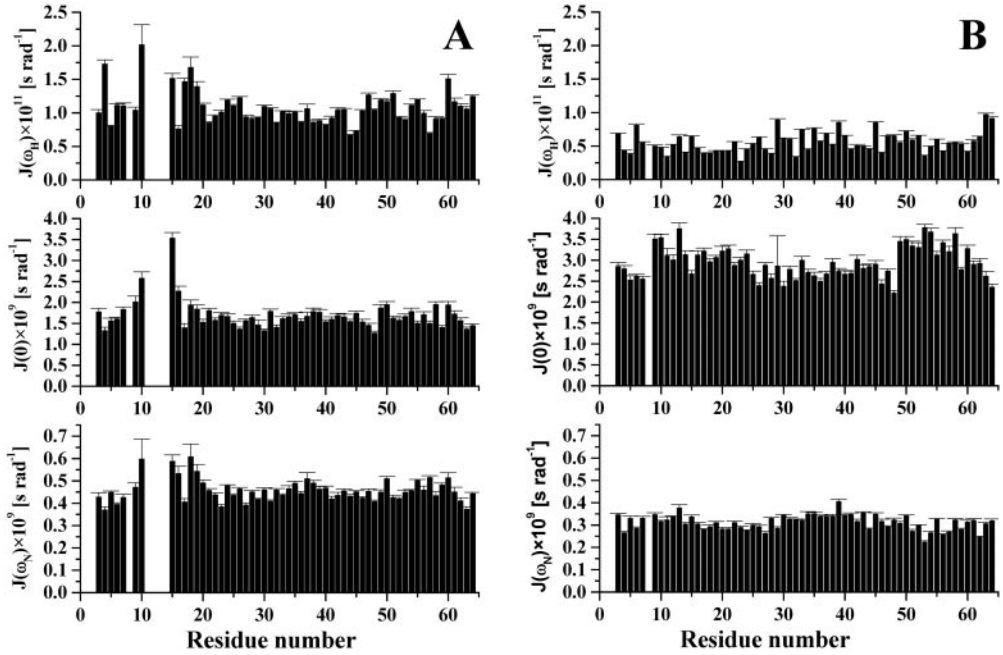

FIG. 2. **Spectral density functions $J(\omega_H)$, $J(0)$, and $J(\omega_N)$ *versus* the residue numbers as obtained from the ^{15}N relaxation data measured at 600 MHz for apo (*A*) and Cu(I)ScAtx1 (*B*).**

family of apoScAtx1 structures are reported in Table I. The structure displays the following secondary structure elements: 2–7 (β1), 16–27 (α1), 31–35 (β2), 39–45 (β3), and 47–60 (α2), in accordance with the $^3J_{HNH\alpha}$ coupling constants, the $d_{\alpha N}(i-1,i)/d_{N\alpha}(i,i)$ ratios and the NOEs patterns. In Fig. 1, the 20 conformers of apoScAtx1 are shown as a tube, whose radius is proportional to the backbone r.m.s.d. of each residue.

^{15}N R_1, R_2, and ^1H-^{15}N NOE values, which provide information on internal mobility, were measured at 600 MHz for all assigned backbone NH resonances. Such average values are 2.46 ± 0.07, 7.09 ± 0.19, and 0.80 ± 0.08 s^{-1}, respectively. The experimental relaxation data are reported in the supplemental material (Fig. 1). The correlation time for molecular reorientation (τ_m), as estimated from the R_2/R_1 ratio, is 4.3 ± 0.3 ns, as expected for a protein of this size in a monomeric state (7). R_1, R_2, and ^1H-^{15}N NOE values were mostly homogeneous along the entire polypeptide sequence, with the exception of some residues located in loop 1 and in the first turn of helix α1, which show larger R_2 and R_1 values. From the spectral density function analysis (Fig. 2*A*), it appears that the apoScAtx1 protein can be considered as a rigid body with only one flexible region involving residues Gln-4, Ile-10, Cys-15, Glu-17, Ala-18, Val-19, and Gly-60, mostly located in loop 1, which have $J(\omega_H)$ significantly higher than average, thus indicating for these residues the presence of local motions in nanosecond to picosecond time scale, *i.e.* faster than the overall protein tumbling rate. In addition to these fast internal motions, slow conformational exchange processes on the millisecond to microsecond time scale affect part of loop 1. Indeed, $J(0)$ values higher than the average are observed for residues Ile-10, Cys-15, and Ala-16 (Fig. 2*A*), which are at the boundaries of residues 11–14 whose NHs signals could not be observed, likely because of line broadening due to conformational exchange processes. Overall, this region comprising the metal-binding motif shows increased backbone flexibility.

Relaxation Measurements, Correlation Time for Reorientation of Cu(I)Atx1, and Evidence of a Dimer—R_1, R_2, and ^1H-^{15}N NOE values were measured at 600-MHz for all assigned backbone NH resonances on a 0.8 mM sample of Cu(I)ScAtx1. The backbone NHs, assigned as in the case of the apo form, are 61 (see below). The average values of R_1, R_2, and ^1H-^{15}N NOE are 1.66 ± 0.14, 10.98 ± 0.40, and 0.78 ± 0.06, respectively. The experimental relaxation data are reported in the supplemental material (Fig. 2). They were essentially homogeneous along the entire polypeptide sequence. The R_2 values show, overall, a sizable increase with respect to apoScAtx1, whereas the R_1 values show a global decrease. From the spectral density function analysis (Fig. 2*B*), it appears that Cu(I)ScAtx1 is inflexible, and even the metal binding region is completely rigid at variance with the apo form. The presence of conformational exchange on the millisecond to microsecond time scale was also evaluated in the copper(I) form via R_2 measurements as a function of τ_{CPMG} length, in order to check if the global increase of R_2 could be due to increased backbone flexibility on the latter time scale. Only residues in the loop regions show conformational exchange, and therefore, the global increase of R_2, coupled with a concomitant global decrease of R_1, implies a copper(I)-dependent change in molecular size. Indeed, the correlation time τ_m, as estimated from the R_2/R_1 ratio, is 7.6 ± 0.7 ns (at 0.8 mM Cu(I)ScAtx1), close to double that of apoScAtx1 (4.3 ± 0.3 ns) and furthermore about double that expected on the basis of the monomeric molecular weight, again consistent with dimeric Cu(I)ScAtx1.

Only one set of resonances is observed in the ^1H-^{15}N HSQC spectrum, indicating that two protein molecules of the dimer interact in a symmetric way producing degenerate resonances for both molecules. The average R_2 and R_1 values and the correlation time τ_m, as well as the chemical shifts, are essentially independent of the protein concentration in the 0.1–0.8 mM range (Table II), indicating that the two molecules are covalently linked. Significantly, addition of an excess of DTT produced a ^1H-^{15}N HSQC spectrum very similar to that of the apo form. R_1, R_2, and τ_m values of DTT-treated Cu(I)ScAtx1 are also similar to those of the apo form. Overall, these data indicate that copper(I) is removed by DTT with the concomitant dissociation of homodimers.

The determination of the rotational diffusion parameters of a protein allows us to analyze the association state in solution by using relaxation data (39). Following this approach, we have calculated the inertia tensors of the structures of both mono-

TABLE II
Average R_1 and R_2 relaxation rates (s^{-1}), ^1H-^{15}N NOEs for amide ^{15}N nuclei measured at 600 MHz for apo and Cu(I)ScAtx1 from Synechocystis PCC 6803

Correlation time for molecular tumbling τ_m (ns) as estimated from the R_2/R_1 ratio is also reported.

	R_1	R_2	τ_m	NOE
		s^{-1}	ns	
ApoScAtx1(0.6 mM)	2.46 ± 0.07	7.09 ± 0.19	4.3 ± 0.3	0.80 ± 0.08
Cu(I)ScAtx1(0.8 mM)	1.66 ± 0.14	10.98 ± 0.40	7.6 ± 0.7	0.78 ± 0.06
Cu(I)ScAtx1(0.3 mM)	1.76 ± 0.10	10.57 ± 0.32	7.2 ± 0.8	
Cu(I)ScAtx1(0.1 mM)	1.93 ± 0.27	11.76 ± 0.24	7.3 ± 0.8	
Cu(I)ScAtx1(0.1 mM) with 1.5 mM DTT	2.55 ± 0.16	8.13 ± 0.28	4.7 ± 0.8	

meric apoScAtx1 and the monomeric/dimeric forms of Cu(I)ScAtx1 (see below). The diffusion tensors of the apo and copper(I) forms (in the latter case by using both dimeric and monomeric structures) were obtained with the program quadric_diffusion (see "Experimental Procedures"). For the apo monomeric form, the calculation indicates a statistically better fit for the relaxation data by using an isotropic diffusion model over an axially symmetric model. Conversely, for a Cu(I) monomeric form the calculations fit better with an axial diffusion model (F statistic $\gg$3). However, a change in the shape of the protein so as to shift the global diffusion model from isotropic to axial is only consistent with a change in the aggregation state induced by copper(I). The relaxation parameters of Cu(I)ScAtx1 are better fitted using a dimeric structure model, that is, when comparing the orientation of the principal components of the axial diffusion tensor with those of the inertia tensors of monomeric and dimeric Cu(I)ScAtx1, we found a very good agreement for the dimeric form, whereas a larger discrepancy is observed for the monomeric form.

Cu(I)ScAtx1 samples have different retention times on size exclusion chromatography in 50 mM phosphate buffer, pH 7.0, in the presence or absence of DTT (23.80 *versus* 21.66 min), whereas the retention time of apoScAtx1 is unaffected by DTT (24.12 min). In comparison, a single holo-ferredoxin fold subdomain of the yeast P_1-type ATPase, Cu(I)-Ccc2a, which is known to retain Cu(I) in the presence of DTT and to be monomeric in both apo and copper(I) forms (40), showed similar retention times in both the presence (24.57 min) and absence (24.73 min) of DTT. This is consistent with Cu(I)ScAtx1 being DTT-labile, and Cu(I)ScAtx1 forming higher M_r (shorter retention time) dimers.

Solution Structure of Cu(I)ScAtx1—ApoScAtx1 was metalated using copper(I) chloride as reported previously (13), thus obtaining a 1:1 copper(I):protein adduct (metal/protein ratio 0.9). Assignments of the resonances of Cu(I)ScAtx1 started from the analysis of the ^1H-^{15}N HSQC maps that allowed the identification of the ^{15}N and ^1HN resonances with different chemical shift with respect to the apo form. From the analysis of ^{15}N-edited three-dimensional NOESY-HSQC and of two-dimensional NOESY and TOCSY maps, sequence-specific assignment of the new resonances was performed. 61 of the expected 63 ^{15}N backbone amide resonances were observed and assigned. The missing backbone NH resonances are those of Met-1 and Thr-2. Totally, the resonances of 97% of nitrogen atoms and 98% of protons were assigned. The ^1H and ^{15}N resonance assignments of the Cu(I) form is reported in supplemental Table 2. Some signals exhibit sizable shift variations between the apo and the copper-bound forms. The largest chemical shift differences, taking into account both ^{15}N and ^1H chemical shifts, occur in the stretches 10–19, 36–41, and 58–64, which mostly comprise loop 1, helix α1, loop 3, and loop 5. Such residues are all located in the vicinity of the copper-binding site, thus indicating that significant structural rearrangements are induced by copper binding.

EXAFS data (13) indicate that one His (His-61 in loop 5) and two Cys (Cys-12 and -15 in loop 1) are involved in copper(I) coordination. ^1H-^{15}N HSQC experiments optimized for the detection of the $^2J_{NH}$ couplings in the imidazole ring were performed on apo and copper(I) forms to investigate the coordination status of His-61 at room temperature in solution (Fig. 3). The resonances of nitrogen atoms coordinated to a metal ion can be easily discriminated from those of the noncoordinated nitrogen atoms on the basis of their chemical shift values (about 220 ppm for the metal-bound nitrogen *versus* 180 or 250 ppm, the two latter values depending on whether the nitrogen is protonated or not (41, 42)). In apoScAtx1, His-61, protonated on $N^{\epsilon 2}$, has chemical shifts of $N^{\delta 1}$ 164.7, $N^{\epsilon 2}$ 243.6, C–$H^{\delta 2}$ 6.31, and C–$H^{\epsilon 1}$ 7.63 ppm. In contrast in Cu(I)ScAtx1, His-61 is protonated on $N^{\delta 1}$, whereas $N^{\epsilon 2}$ is coordinated to the copper ion. The chemical shifts for $N^{\delta 1}$, $N^{\epsilon 2}$, C–$H^{\delta 2}$, and C–$H^{\epsilon 1}$ are 168.9, 219.0, 6.37, and 7.60 ppm, respectively. The chemical shift of $N^{\epsilon 2}$ is consistent with the presence of a coordination bond between $N^{\epsilon 2}$ of His-61 and copper (22), in accordance with the EXAFS data (13).

2300 NOE cross-peaks have been assigned and integrated, providing 1429 unique upper distance limits, of which 1099 are meaningful. 43 ϕ angle constraints were used in structure calculations. Initially, the structure calculations were performed assuming a monomeric state. In these calculations, upper distance limits between the copper(I) ion and the sulfur atoms of Cys-12 and -15 and $N^{\epsilon 2}$ of His-61 were applied in the calculations. After restrained energy minimization with the AMBER program on each of the 20 lowest target function structures, obtained from DYANA calculations, the r.m.s.d. for backbone and heavy atoms to the mean structure (for residues 3–64) is 0.31 (with a variability of 0.07 Å) and 0.70 (with a variability of 0.04 Å), respectively. The penalty for distance constraints is 0.17 ± 0.04 Å^2. The low penalty value indicates that *all* applied constraints can well satisfy a monomeric structure (Fig. 4*A*). Calculations were then pursued with either of these conditions: (i) the two subunits are linked by a coordination bond between His-61 of one subunit and copper(I) of the other subunit (His-linked model); (ii) the two subunits are linked by a coordination bond between Cys-12 or -15 of one subunit and copper(I) of the other subunit (Cys-linked model). A dinuclear copper(I) center with bridging sulfur atoms, as proposed at low temperature from EXAFS data CopZ of *B. subtilis* (43), should be discarded as EXAFS data, in the present case, did not reveal a short copper-copper distance (13). When the $N^{\epsilon 2}$ of the imidazole ring of His-61 belonging to one subunit was bound to the copper(I) ion of the other subunit with an upper distance limit of 2.2 Å, the average target function is 0.23 ± 0.04 Å^2 and backbone r.m.s.d. is 0.54 (with a variability of 0.09 Å). Again, all the experimental data are consistent with a dimeric His-linked model (Fig. 4*B*).

The Cys-linked structural models were obtained with DYANA calculations with the S^{γ} of Cys-12 or -15 belonging to one subunit with an upper distance limit of 2.5 Å to the copper(I) ion of the other subunit. In the case of Cys^{15}-linked model, DYANA calculations give an increased target function value of

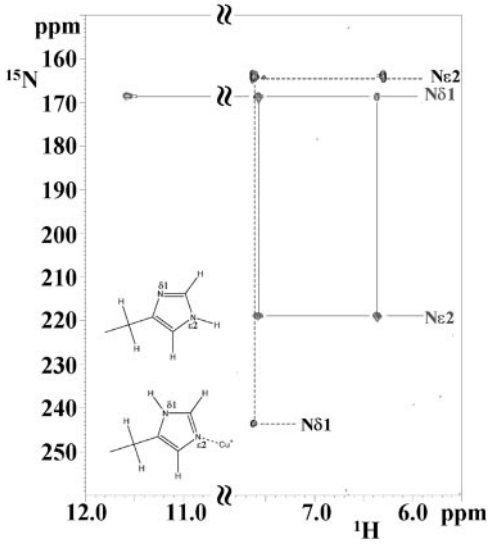

FIG. 3. **^{1}H ^{15}N HSQC spectra optimized for the detection of $^{2}J_{NH}$ of histidine rings, recorded on apo (*dotted line*) and Cu(I)ScAtx1 (*straight line*) at protein concentrations of 0.6 and 0.8 mM, respectively.** The spectra were collected at 298 K and pH 7, on a spectrometer equipped with cryo-probe and operating at 500 MHz. The tautomeric species of His ring of apo and copper(I) forms are also depicted.

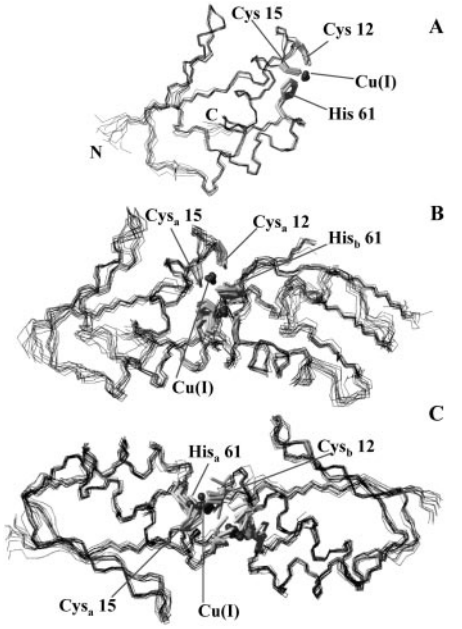

FIG. 4. **Representation of the bundle of the 10 lowest energy conformers of Cu(I)ScAtx1 in the monomeric (*A*), homodimeric His-61-linked (*B*), and homodimeric Cys-12-linked (*C*) forms after best fit superposition of the backbone atoms of both subunits.** The side chains of His-61, Cys-12, Cys-15, and the Cu(I) ions are also shown.

0.82 ± 0.15 Å^2, and the family structures display too short copper(I)-copper(I) distances (from 1.0 to 2.5 Å), inconsistent with the EXAFS results (13). Therefore, we exclude the latter structural model. On the contrary, the Cys^{12}-linked model has a low average target function value of 0.23 ± 0.04 Å^2 and a backbone r.m.s.d. values of 0.80 (with a variability of 0.10 Å). This is also a structural model consistent with the experimental restraints (Fig. 4*C*). When a subunit of the His-linked model was superimposed to a subunit of the Cys-linked model, the subunits are essentially identical (r.m.s.d. 0.5 Å), but the reciprocal orientation of the other domains is significantly different. In particular, the Cys-linked dimeric structural rearrangement is almost linear, whereas the long axes of the two domains in the His-linked model form an angle of 40° (Fig. 4, *B* and *C*). In both cases, the interface of homodimer between the two subunits comprises residues located around loop 1 and at the carboxyl-terminal region, which are mainly composed of small hydrophilic residues as Thr, Ala, and Gly. As a result, the experimental restraints, which produce high resolution structures, are completely consistent with both dimeric structures. In addition, both dimeric His- and Cys^{12}-linked models indicate a long copper-copper distances of 5.5 ± 0.1 and 6.1 ± 0.5 Å, respectively, which account for the absence of a second shell (Cu-Cu) contribution to the EXAFS spectrum (Fig. 4, *B* and *C*) (13).

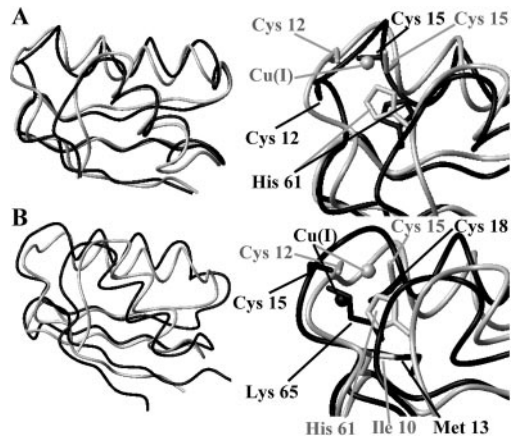

FIG. 5. **Comparison of the backbone of the monomeric Cu(I)ScAtx1 (*light gray*) with apoScAtx1 (*black*) (*A*) and Cu(I)Atx1 of *S. cerevisiae* (*black*) (*B*).** On the *right panel*, the copper(I) ion and the Cys and His residues involved in copper binding and other relevant residues in the metal-binding loop are shown.

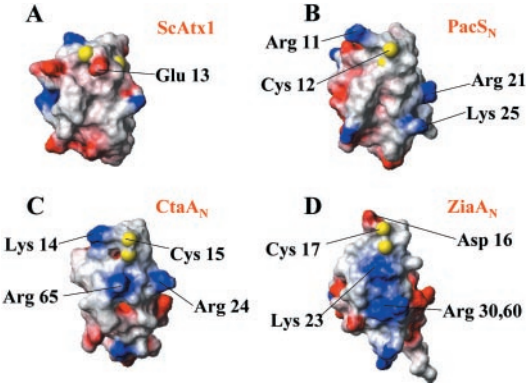

FIG. 6. **Electrostatic potential surface of ScAtx1 (*A*) and, of the structural models of PacS$_N$ (*B*), CtaA$_N$ (*C*), and ZiaA$_N$ (*D*).** The positively and negatively charged and neutral amino acids are represented in *blue, red,* and *white*, respectively. The positions of Cys residues are identified as *yellow spheres* and other charged residues are also indicated. Structural models for the sequences of PacS$_N$, CtaA$_N$, and ZiaA$_N$ were calculated using the solution structure of the first amino-terminal domain of CopA from *B. subtilis* (62) as template.

The statistical analysis of the REM families of monomeric and dimeric Cu(I)ScAtx1 structures are reported in supplemental Tables 3–5. All structures display the same secondary structure elements, as in the apo form but with different lengths as follows: 3–7 (β1), 12–27 (α1), 31–35 (β2), 39–44 (β3), 48–60 (α2). Cys-12 and -15 are in helix α1, whereas they are in a loop in the apo form.

It is noted that the back calculated NOEs (within a 5-Å distance) from the two dimeric models in the metal ligand region are the same and are also the same for the monomer. This prevents discrimination between the two dimers and pre-

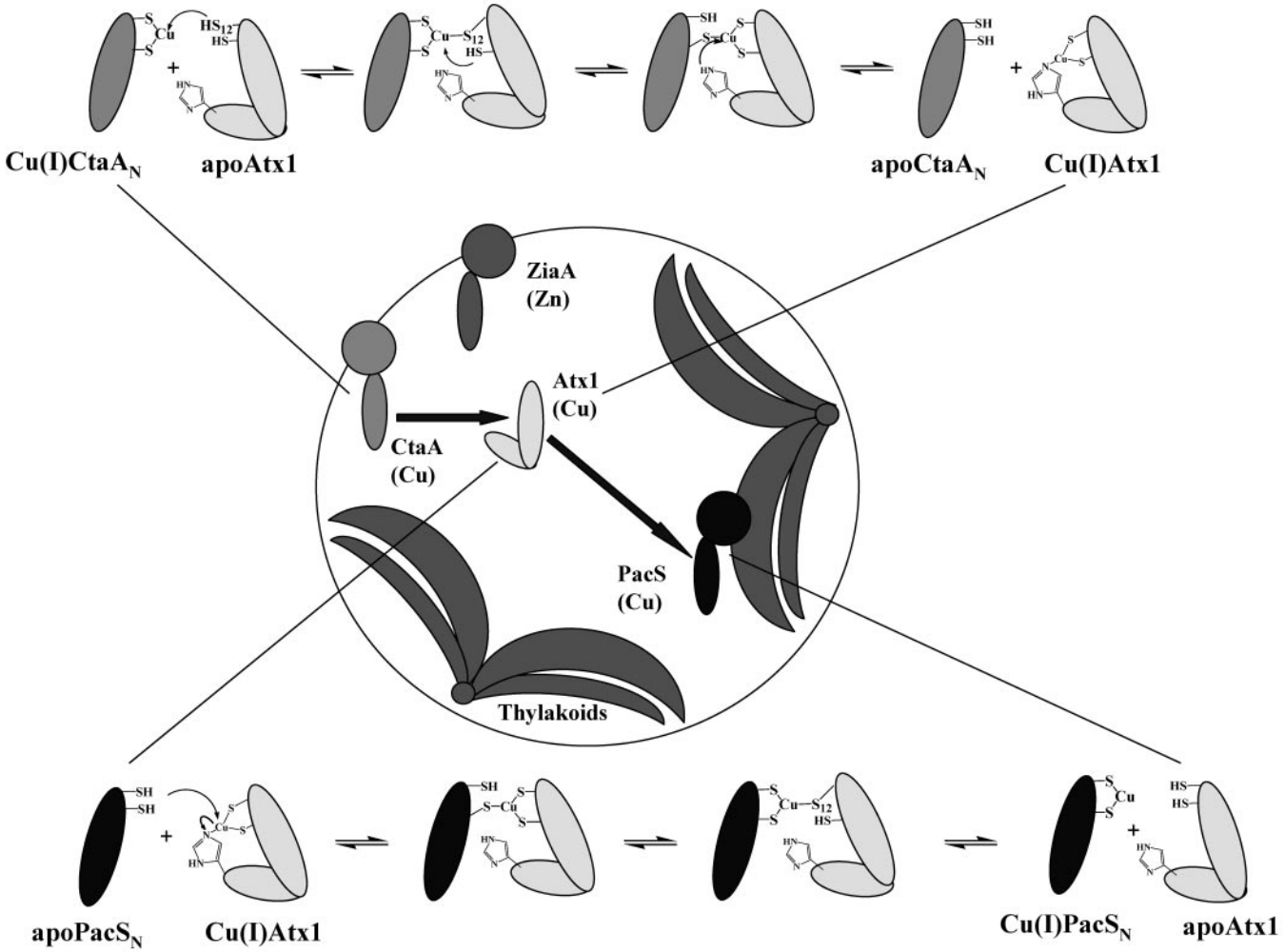

FIG. 7. **Proposed pathway for copper transfer from CtaA to PacS through ScAtx1.** This model implies that the order of copper(I) association with ScAtx1 ligands 1) Cys-12, 2) Cys-15, and finally 3) His-61 during acquisition from $CtaA_N$ with the converse order of ligand release upon interaction with $PacS_N$.

cludes the application of investigative techniques based on ^{13}C-labeled/unlabeled samples (44–46).

DISCUSSION

The overall folding of the copper-free (Fig. 1) and the three copper-bound forms of ScAtx1 (Fig. 4) are almost identical. All of the secondary structure elements are well superimposed with the exception of helix α1 which is shorter by one turn in the apo form (Fig. 5*A*). The secondary structure elements are organized into a $\beta\alpha\beta\beta\alpha$ fold, the final β strand (β4) found in related copper metallochaperones (47–49) being essentially absent, although a few backbone NOE cross-peaks typical for an antiparallel β-sheet are observed between Thr-6, Val-7, Glu-64, and Val-63 (see supplemental material). Localized surface charge indicates how ScAtx1 may recognize soluble domains of copper ATPases but avoid a zinc ATPase (Fig. 6). The resulting specificities of these partnerships, rather than the inherent metal-binding preferences of the ATPases, may select which metals become available for transport. Metal-ligand arrangements of Cu(I)ScAtx1 (Figs. 3 and 4) coupled with observed backbone motions provide insight into how copper ions can pass from the plasma membrane to an intracellular compartment along a ligand gradient, without release into the cytosol (Fig. 7).

Cys-12 and -15 are part of an α-helix in Cu(I)ScAtx1 but not in apoScAtx1 (Fig. 5*A*). A similar observation has been made for Atx1 from *Saccharomyces cerevisiae* (47). The backbone conformation of the carboxyl-terminal tail changes between the apo and copper(I) forms (Fig. 5*A*); however, His-61 in this region shows NOEs with hydrophobic residues Ile-10, Val-19, Ala-59, and Ile-56 in both apo- and Cu(I)ScAtx1 (although less in the former), suggesting that His-61 maintains hydrophobic packing. Mobility studies on apoScAtx1 show greater backbone flexibility in loop 1 relative to the region containing His-61, and Cu(I) induces structural and dynamic change mostly around the Cys motif.

The side chain of Ile-10 in loop 1 maintains the same orientation in both apo and copper(I) forms, interacting with the hydrophobic residues Leu-36 in loop 3 and/or Val-34 in strand β2. Most interestingly, Ile-10 takes the place of a methionine residue that is highly conserved in other soluble copper metallochaperones as well as in the amino-terminal soluble domains of membrane-bound ATPases (50), supporting the idea that this methionine could act as a hydrophobic tether that anchors the metal-binding loop via hydrophobic interactions (50, 51).

Copper-mediated dimerization of ScAtx1 has analogy to the observed Cu(I)-dependent aggregation of CopZ from *Enterococcus hirae*, which was speculated to form Cu(I)-CopZ dimers (49). In contrast, CopZ from *B. subtilis* (i) is dimeric at millimolar concentrations in apo and copper(I) forms, (ii) shows dimerization of both forms that is concentration-dependent, and (iii) does not release copper(I) from the holocomplex to DTT (43). The present characterization of Cu(I)ScAtx1 points at a

stable homodimer where the two subunits are linked through coordination bonds between the copper(I) ions and ligands of the two subunits, at variance with *B. subtilis* CopZ where the subunits interact through nonspecific electrostatic or hydrophobic interactions. The functional relevance of dimerization remains to be addressed, although the apo form is clearly monomeric, and it is speculated that dimerization may only occur at high concentrations *in vitro*. Structural models for monomers are equally compatible with the NOEs as dimeric forms, consistent with minimal contact occurring between the subunits beyond the shared ligands plus minimal structural rearrangement upon dimerization.

Structural data, including low temperature EXAFS when available (43, 52–54), show that a third donor atom enters the $Cu(I)S_2$ coordination sphere of various eukaryotic and bacterial copper(I) chaperones for P_1-type ATPases. In CopZ from *B. subtilis*, the reductant DTT may provide the third donor *in vitro* (43). This is consistent with digonal copper(I) tending to expand its coordination number. EXAFS (13) and NMR data imply that ScAtx1 is an exception with an endogenous His residue forming a third coordination bond with copper(I), in addition to two *Cys*, and here we show that $N^{\epsilon 2}$ of His-61 is the third ligand (Fig. 3). This submolecular variant in ScAtx1 could either have been selected as an adaptation to some atypical subcellular role(s) peculiar to ScAtx1, and perhaps also to Sco1, which has similar Cu(I) coordination (55), or be an ancestral relic substituted by nonbonding stabilization of digonal copper sites via Lys in analogous eukaryotic proteins.

In all eukaryotic organisms in the position corresponding to His-61, there is a fully conserved Lys (Lys-65 in *S. cerevisiae*). Lys-65, although not bound (47, 52), points toward the copper(I) ion with an orientation of its side chain similar to that of His-61 (Fig. 5*B*). Additionally, conserved hydrophobic residues, Met-13 in Atx1 and Ile-10 in ScAtx1, display the same orientation in both Cu(I) structures, interacting with a conserved Leu in loop 3, thus conferring a similar bend of loop 1 toward the core of the protein (Fig. 5*B*).

In homologous systems, such as yeast Atx1/Ccc2 and CopZ/CopA from *B. subtilis*, where the chaperone also delivers copper(I) to soluble domains of P_1-type ATPases, the partners are characterized by well defined complementary surface charges that are responsible for long range interactions (4, 7). Short range hydrophobic interactions are also operative and signal copper occupancy of the chaperone (56). Most intriguing, a model of the soluble parts of PacS ($PacS_N$) does not display any extensive electrostatic complementary surface with ScAtx1 (Fig. 6). The soluble parts of CtaA ($CtaA_N$) also do not display well defined electrostatic complementary surfaces with ScAtx1 (Fig. 6), but these proteins do interact *in vivo,* and it is assumed that CtaA loads copper onto ScAtx1 (3). The proteins that supply copper to CopZ in other bacteria remain to be identified, and although yeast Atx1 can interact with a domain of a Ctr family copper importer *in vitro* (57), this is not essential for Atx1 function *in vivo* (58, 59). It has been hypothesized that His-61 in ScAtx1 may influence the directionality of copper(I) transfer with respect to the two different P_1-type ATPases, PacS and CtaA (60). Greater structural flexibility of loop 1 suggests that one or other Cys residue of apoScAtx1 is more likely to first invade the copper-loaded site of $CtaA_N$, as proposed for Atx1 and Ccc2a from *S. cerevisiae* (52), rather than His-61. Dimer models (Fig. 4) implicate Cys-12, not Cys-15, as the pioneer. Subsequently, entrance of His-61 into the copper(I) site will nonetheless promote copper(I) acquisition by the copper metallochaperone with the concomitant displacement of CtaA. Lys-65 in the human Atx1-target protein complex is suggested to counterbalance the negative charge from the two target cysteinates of the protein partner (6), thus rendering the coordination environment in the target protein slightly more favorable than in the chaperone. His-61 can render the copper(I) coordination environment more favorable in ScAtx1 than in CtaA because of formation of a coordination bond with $N^{\epsilon 2}$ of His-61. How is this process reversed upon interaction with PacS?

DTT is able to remove copper(I) from ScAtx1, at variance with Atx1 from *S. cerevisiae* (52), and it is possible that the electrostatic field around the metal ion in ScAtx1 increases lability. When Cu(I)ScAtx1 approaches apoPacS, it is speculated that His-61 is somehow displaced from the coordination sphere allowing one of the two cysteine residues of PacS to encroach into a shared copper(I) site as proposed for Atx1/Ccc2a. Thus the favored order of copper(I) association with ScAtx1 ligands is 1) Cys-12, 2) Cys-15, and finally 3) His-61 at acquisition from CtaA with the converse order of release at interaction with PacS (Fig. 7).

Localized negative charge from Glu-13, close to the metal-binding Cys residues of ScAtx1, could support interaction with complementary Arg and Lys in equivalent locations in PacS and CtaA (Fig. 6). Lys/Arg residues are only adjacent to these Cys in metal-transporting P_1-type ATPases of *Synechococcus* PCC 7942, *Synechocystis* PCC 6803, and *Caulobacter crescentus* (50). In the latter case, the ATPase is a member of the Fix operon that includes cytochrome *c* oxidase (50) and serves to activate cytochrome *c* oxidase (61). This surface feature thus correlates with roles in copper supply to cytochrome *c* oxidase in aquatic bacteria.

In summary, trafficking via sequential ligand exchange (Fig. 7) will prevent copper from entering thermodynamic traps, adventitious high affinity copper(I) sites, while *en route* to thylakoids. Such sites are likely to include ones that should be occupied by other metals but that nonetheless have tighter affinity for copper(I). The soluble domain of the zinc exporter ZiaA contains such a site (11). The presence of Asp-16 (rather than Lys/Arg) adjacent to the first Cys of ZiaA may crucially discourage ScAtx1-ZiaA interaction and ultimately serve to prevent copper from erroneously trafficking to the transporter for zinc.

REFERENCES

1. Bogsch, E., Brink, S., and Robinson, C. (1997) *EMBO J.* **16,** 3851–3859
2. Tottey, S., Rich, P. R., Rondet, S. A. M., and Robinson, N. J. (2001) *J. Biol. Chem.* **276,** 19999–20004
3. Tottey, S., Rondet, S. A., Borrelly, G. P., Robinson, P. J., Rich, P. R., and Robinson, N. J. (2002) *J. Biol. Chem.* **277,** 5490–5497
4. Banci, L., Bertini, I., Ciofi-Baffoni, S., Del Conte, R., and Gonnelli, L. (2003) *Biochemistry* **42,** 1939–1949
5. Radford, D. S., Kihlken, M. A., Borrelly, G. P. M., Harwood, C. R., Le Brun, N. E., and Cavet, J. S. (2003) *FEMS Microbiol. Lett.* **220,** 105–112
6. Wernimont, A. K., Huffman, D. L., Lamb, A. L., O'Halloran, T. V., and Rosenzweig, A. C. (2000) *Nat. Struct. Biol.* **7,** 766–771
7. Arnesano, F., Banci, L., Bertini, I., Cantini, F., Ciofi-Baffoni, S., Huffman, D. L., and O'Halloran, T. V. (2001) *J. Biol. Chem.* **276,** 41365–41376
8. Kanamaru, K., Kashiwagi, S., and Mizuno, T. (1994) *Mol. Microbiol.* **13,** 369–377
9. Phung, L. T., Ajlani, G., and Haselkorn, R. (1994) *Proc. Natl. Acad. Sci. U. S. A.* **91,** 9651–9654
10. Thelwell, C., Robinson, N. J., and Turner-Cavet, J. S. (1998) *Proc. Natl. Acad. Sci. U. S. A.* **95,** 10728–10733
11. Borrelly, G. P. M., Rondet, S. A. M., Tottey, S., and Robinson, N. J. (2004) *Mol. Microbiol.,* in press
12. Changela, A., Chen, K., Xue, Y., Holshen, J., Outten, C. E., O'Halloran, T. V., and Mondragon, A. (2003) *Science* **301,** 1383–1387
13. Borrelly, G. P. M., Blindauer, C. A., Schmid, R., Butler, C. S., Cooper, C. E., Harvey, I., Sadler, P. J., and Robinson, N. J. (2004) *Biochem. J.* **378,** 293–297
14. Griesinger, C., Otting, G., Wüthrich, K., and Ernst, R. R. (1988) *J. Am. Chem. Soc.* **110,** 7870–7872
15. Macura, S., Wüthrich, K., and Ernst, R. R. (1982) *J. Magn. Reson.* **47,** 351–357
16. Marion, D., and Wüthrich, K. (1983) *Biochem. Biophys. Res. Commun.* **113,** 967–974
17. Palmer, A. G., III, Cavanagh, J., Wright, P. E., and Rance, M. (1991) *J. Magn. Reson.* **93,** 151–170
18. Kay, L. E., Marion, D., and Bax, A. (1989) *J. Magn. Reson.* **84,** 72–84
19. Schleucher, J., Schwendinger, M., Sattler, M., Schmidt, P., Schedletzky, O.,

Glaser, S. J., Sorensen, O. W., and Griesinger, C. (1994) *J. Biomol. NMR* **4,** 301–306
20. Vuister, G. W., and Bax, A. (1993) *J. Am. Chem. Soc.* **115,** 7772–7777
21. Archer, S. J., Ikura, M., Torchia, D. A., and Bax, A. (1991) *J. Magn. Reson.* **95,** 636–641
22. Eijkelenboom, A. P., Van den Ent, F. M., Vos, A., Doreleijers, J. F., Hard, K., Tullius, T. D., Plasterk, R. H., Kaptein, R., and Boelens, R. (1997) *Curr. Biol.* **7,** 739–746
23. Eccles, C., Güntert, P., Billeter, M., and Wüthrich, K. (1991) *J. Biomol. NMR* **1,** 111–130
24. Herrmann, T., Güntert, P., and Wüthrich, K. (2002) *J. Mol. Biol.* **319,** 209–227
25. Güntert, P., Mumenthaler, C., and Wüthrich, K. (1997) *J. Mol. Biol.* **273,** 283–298
26. Pearlman, D. A., Case, D. A., Caldwell, J. W., Ross, W. S., Cheatham, T. E., Ferguson, D. M., Seibel, G. L., Singh, U. C., Weiner, P. K., and Kollman, P. A. (1997) *AMBER*, *Version 5.0*, University of California, San Francisco
27. Banci, L., Bertini, I., Cramaro, F., Del Conte, R., and Viezzoli, M. S. (2002) *Eur. J. Biochem.* **269,** 1905–1915
28. Laskowski, R. A., Rullmann, J. A. C., MacArthur, M. W., Kaptein, R., and Thornton, J. M. (1996) *J. Biomol. NMR* **8,** 477–486
29. Koradi, R., Billeter, M., and Wüthrich, K. (1996) *J. Mol. Graphics* **14,** 51–55
30. Farrow, N. A., Muhandiram, R., Singer, A. U., Pascal, S. M., Kay, C. M., Gish, G., Shoelson, S. E., Pawson, T., Forman-Kay, J. D., and Kay, L. E. (1994) *Biochemistry* **33,** 5984–6003
31. Peng, J. W., and Wagner, G. (1994) *Methods Enzymol.* **239,** 563–596
32. Mulder, F. A., Van Tilborg, P. J., Kaptein, R., and Boelens, R. (1999) *J. Biomol. NMR* **13,** 275–288
33. Grzesiek, S., and Bax, A. (1993) *J. Am. Chem. Soc.* **115,** 12593–12594
34. Peng, J. W., and Wagner, G. (1992) *J. Magn. Reson.* **98,** 308–332
35. Brüschweiler, R., Liao, X., and Wright, P. E. (1995) *Science* **268,** 886–889
36. Mandel, M. A., Akke, M., and Palmer, A. G., III (1995) *J. Mol. Biol.* **246,** 144–163
37. Kay, L. E., Torchia, D. A., and Bax, A. (1989) *Biochemistry* **28,** 8972–8979
38. Tjandra, N., Feller, S. E., Pastor, R. W., and Bax, A. (1995) *J. Am. Chem. Soc.* **117,** 12562–12566
39. Tsan, P., Hus, J. C., Caffrey, M., Marion, D., and Blackledge, M. (2000) *J. Am. Chem. Soc.* **122,** 5603–5612
40. Huffman, D. L., and O'Halloran, T. V. (2000) *J. Biol. Chem.* **275,** 18611–18614
41. Pelton, J. G., Torchia, D. A., Meadow, N. D., and Roseman, S. (1993) *Protein Sci.* **2,** 543–558
42. Chen, Y.-L., Park, S., Thornburg, R. W., Tabatabai, L. B., and Kintanar, A. (1995) *Biochemistry* **34,** 12265–12275
43. Banci, L., Bertini, I., Del Conte, R., Mangani, S., and Meyer-Klaucke, W. (2003) *Biochemistry* **8,** 2467–2474
44. Ikura, M., and Bax, A. (1992) *J. Am. Chem. Soc.* **114,** 2433–2440
45. Folkers, P. J. M., Folmer, R. H. A., Konings, R. N. H., and Hilbers, C. W. (1993) *J. Am. Chem. Soc.* **115,** 3798–3799
46. Zwahlen, C., Legault, P., Vincent, S. J. F., Greenblatt, J., Konrat, R., and Kay, L. E. (1997) *J. Am. Chem. Soc.* **119,** 6711–6721
47. Arnesano, F., Banci, L., Bertini, I., Huffman, D. L., and O'Halloran, T. V. (2001) *Biochemistry* **40,** 1528–1539
48. Banci, L., Bertini, I., Del Conte, R., Markey, J., and Ruiz-Dueñas, F. J. (2001) *Biochemistry* **40,** 15660–15668
49. Wimmer, R., Herrmann, T., Solioz, M., and Wüthrich, K. (1999) *J. Biol. Chem.* **274,** 22597–22603
50. Arnesano, F., Banci, L., Bertini, I., Ciofi-Baffoni, S., Molteni, E., Huffman, D. L., and O'Halloran, T. V. (2002) *Genome Res.* **12,** 255–271
51. Banci, L., Bertini, I., Ciofi-Baffoni, S., Huffman, D. L., and O'Halloran, T. V. (2001) *J. Biol. Chem.* **276,** 8415–8426
52. Pufahl, R., Singer, C. P., Peariso, K. L., Lin, S.-J., Schmidt, P. J., Fahrni, C. J., Cizewski Culotta, V., Penner-Hahn, J. E., and O'Halloran, T. V. (1997) *Science* **278,** 853–856
53. Cobine, P. A., George, G. N., Jones, C. E., Wickramasinghe, W. A., Solioz, M., and Dameron, C. T. (2002) *Biochemistry* **41,** 5822–5829
54. Ralle, M., Lutsenko, S., and Blackburn, N. J. (2003) *J. Biol. Chem.* **278,** 23163–23170
55. Nittis, T., George, G. N., and Winge, D. R. (2001) *J. Biol. Chem.* **276,** 42520–42526
56. Banci, L., Bertini, I., and Del Conte, R. (2003) *Biochemistry* **42,** 13422–13428
57. Xiao, Z., and Wedd, A. G. (2002) *Chem. Commun.* **6,** 588–589
58. Puig, S., and Thiele, D. J. (2002) *Curr. Opin. Chem. Biol.* **6,** 171–180
59. Rensing, C., Ghosh, M., and Rosen, B. P. (1999) *J. Bacteriol.* **181,** 5891–5897
60. Cavet, J. S., Borrelly, G. P., and Robinson, N. J. (2003) *FEMS Microbiol. Rev.* **27,** 165–181
61. Preisig, O., Zufferey, R., and Hennecke, H. (1996) *Arch. Microbiol.* **165,** 297–305
62. Banci, L., Bertini, I., Ciofi-Baffoni, S., Gonnelli, L., and Su, X. C. (2003) *J. Mol. Biol.* **331,** 473–484

Solution Structures of a Cyanobacterial Metallochaperone: INSIGHT INTO AN ATYPICAL COPPER-BINDING MOTIF

Lucia Banci, Ivano Bertini, Simone Ciofi-Baffoni, Xun-Cheng Su, Gilles P. M. Borrelly and Nigel J. Robinson

J. Biol. Chem. 2004, 279:27502-27510.
doi: 10.1074/jbc.M402005200 originally published online April 8, 2004
